Available online at www.eccomasproceedia.org
Eccomas Proceedia COMPDYN (2017) 4607-4622

ECCOMAS
Proceedia

COMPDYN 2017
6th ECCOMAS Thematic Conference on
Computational Methods in Structural Dynamics and Earthquake Engineering
M. Papadrakakis, M. Fragiadakis (eds.)
Rhodes Island, Greece, 15–17 June, 2017

SIMPLIFIED NUMERICAL MODELING STRATEGIES OF DEEP VIBRATORY COMPACTION

Maximilian Schmitter[1], **Christoph Adam**[2]

[1] Unit of Applied Mechanics
University of Innsbruck, Innsbruck, Austria
e-mail: maximilian.schmitter@uibk.ac.at

[2] Unit of Applied Mechanics
University of Innsbruck, Innsbruck, Austria
e-mail: christoph.adam@uibk.ac.at

Keywords: Soil Dynamics, Deep Vibratory Compaction, Current State Simulation, Parameter Identification, Numerical Modeling

Abstract. *In this paper different simplified approaches for numerical simulation of deep vibratory compaction are presented. In the first approach, modal analysis yields the mode shapes and natural frequencies of a planar soil model, with the objective of reducing the degrees of freedom of the soil continuum in a subsequent response history analysis considering only the most dominate modes. Based on the maximum elastic strain energy per mode criterion, the most dominant modes excited by a rotating force are identified, revealing that the most dominant natural frequencies are clustered around multiples of the excitation frequency. It is also shown that* $1.4\,\%$ *of the modes contribute to* $80\,\%$ *of the total strain energy. The second study addresses modeling of vibro-soil interaction, approximating the soil as three-dimensional planar circular section and the vibratory as rigid cylinder rotating in the hole at the soil center. To the surfaces of the two bodies potentially in contact, a contact formulation is assigned. The outcomes of the numerical simulations on this finite element model serve as input for system identification of the soil parameters varying with time due to the compaction process. The underlying lumped parameter model is composed of two discrete spring-dashpot systems and a lumped mass subjected to a rotating force. The contact force can be reasonably identified, however, the utilized mapping algorithm for identification of the time varying soil parameter needs further investigation.*

Peer-review under responsibility of the organizing committee of COMPDYN 2017.
doi: 10.7712/120117.5747.17293

1 INTRODUCTION

Since more than five decades *deep vibratory compaction* has been used to compact non-cohesive granular soil media of considerable depth [14]. The deep vibratory compaction device consists of the vibrator, which is attached to a crane. Inside the vibrator an eccentric rotating mass generates horizontal dynamic forces. As depicted in Fig. 1, *deep vibratory compaction* is

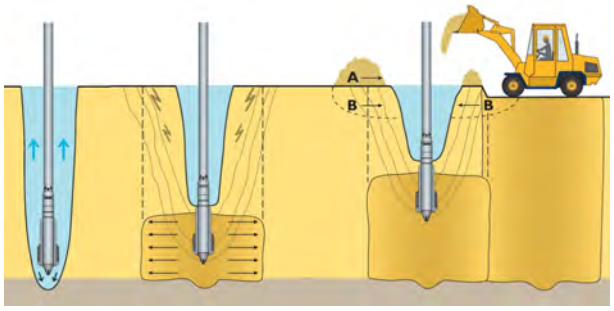

Figure 1: Sketch of soil densification by means of *deep vibratory compaction* [11].

conducted in two stages. In the first stage, the vibrator with rotating mass and high volume water jets at the tip penetrates the soil, taking advantage of the vibrator self-weight, up to the desired depth of compaction. Depending on the utilized crane, additional downward and upward forces accelerate the penetration. From the point of view of mechanical science, the processes at this stage can be explained by means of cavity expansion theories, see e.g. [20]. In the subsequent prescribed stepwise periodical upward motion of the vibratory with simultaneously prescribed mass flow rate of water at the vibrator tip, the adjacent soil media is stepwise compacted. At each step the compaction process is completed when an a priori defined limit value of the power consumption (measured in ampere) is reached. With this kind of intuitive compaction control, in general, reliable soil densification is achieved.

However, there is a demand on a more objective compaction control procedure based on physically quantifiable parameters, such as the dynamic response of the compaction device or of the adjacent soil surface, which would facilitate a fully automated compaction process yielding to more homogeneously compacted subsoil. This procedure should be based on data continuously recorded during compaction, and thus, simultaneous adjustment of operational parameters such as the excitation frequency of the vibratory would be possible. For near-surface compaction by means of vibratory rollers, such a method, i.e. the continuous compaction control (CCC) method, is available [1]. Since launching more than two decades ago, it has become the state of the art control method for roller compaction application. In an attempt to close the gap, Wehr [18] proposed a method for optimal compaction control of deep vibratory compaction.

More recently, a research consortium with members from industry (Keller Grundbau GmbH, Vienna Consulting Engineers ZT GmbH) and academia (TU Wien - Institute of Geotechnics, University of Innsbruck - Unit of Applied Mechanics) was founded, aiming at developing a physically based and reliable compaction control method for deep vibratory compaction. In a project [7] funded by the Austrian Research Promotion Agency (FFG) this research consortium pursues this goal based on in-situ experimental and numerical investigations of deep vibratory compaction.

This papers reports on both simplified and more elaborate, however, feasible numerical modeling efforts of deep vibratory compaction, conducted within the aforementioned research project. The overall goal is to quantify the dynamic behavior of the vibrator-soil interaction system

and the evolution of the compacted soil domain.

In the literature, for *vibro replacement stone columns*, a method similar deep vibratory compaction, several simplified analytical and numerical models have been developed in an effort to estimate the ultimate bearing capacity respectively the magnitude of consolidation settlement of the improved soil. An overview on these studies is found in [13]. Vibratory displacement and vibratory compaction methods used in different soil types rely on a similar rotating vibrator. Both methods have in common that a detailed numerical simulation of the compaction process is extremely demanding in terms of modeling and computational costs, because of three-dimensional dynamic excitation, nonlinear interaction between vibrator and soil, soil liquefaction, soil fluidization and subsequent soil compaction, etc. To reduce the computational effort, for instance, Kessler et al. [12] simulated numerically vibratory compaction using an axial-symmetric thin planar soil section, and compared the outcomes with the ones of a full three-dimensional numerical model. In this approach, due to the axial-symmetric setup, the vibrator model performs a pulsating motion, and therefore, shear distortion of the soil cannot be reproduced although this effect contributes significantly to soil compaction [10]. Cudmani et al. [3] used a hypoplastic infinite cylindrical cavity soil model with a prescribed radial stress component to evaluate the cone penetration resistance after compaction. Based on a planar soil section similar the one used in [12], in [2] elastic strain paths were derived that served as input for a strain excited single element simulation with assigned hypoplastic constitutive law. In [2] the compaction distribution in radial direction was predicted in agreement to the common soil densification hypothesis (e.g. [6, 17]). In the work of Qiu and Hamann [16, 9], a full three-dimensional model of the vibrator-soil interaction system was created to simulate the vibrator penetration (pile installation), using an elaborate coupled Lagrangian and Eulerian displacement field formulation and hypoplastic soil properties. The effect of different excitation frequency and vibrator displacement amplitudes on the void ratio in the subsoil was also investigated.

In the past in-situ experiments have been conducted to reveal the underlying dynamic processes of *deep vibratory compaction*. For instance, in an in-situ test series Wehr [18] varied the excitation frequency of the vibrator to identify optimal conditions for deep vibratory compaction. From his studies Wehr concluded that at a certain frequency the vibrator is in a state of resonance. However, it is still controversially discussed if vibrator resonance is related to soil response amplification and consequently to optimal soil compaction, due to complex interaction and nonlinear material behavior. Small scaled tests were conducted in [15], emphasizing optimal compaction control as proposed in [18]. Fellin et al. [5] estimated the increase of soil compaction based on a hybrid approach of experimental and numerical simulations. They identified parameters for a simple lumped parameter model of the vibrator-soil interaction system from in-situ data of vibratory displacement and phase delay between excitation and vibratory response.

In the present contribution, two different numerical approaches of different elaboration are used to study different aspects of this demanding problem. In the first study a simplified two-dimensional planar model of the vibrator-soil system is subjected to modal analysis, aiming at synthesizing dominant modes vulnerable to specific excitation of the vibrator. Since the soil is assumed to behave linear elastic, this simulation represents a current state description of the system at specific time instants during the compaction process. The second study addresses online time-variant evaluation of soil properties based on recorded response data and a simplified inverse lumped parameter model, similar to [5]. An algorithm based on *Wolf's cone model* [19] is used to map lumped parameter data to feasible soil parameters.

2 DOMINANT MODES OF A PLANAR SOIL SECTION

Numerical analysis of wave propagation in the infinite three-dimensional halfspace is prohibitively computationally expensive, even for a linear time-invariant system. One possibility to reduce the computational effort is the application of modal analysis, considering only modes that contribute significantly to the dynamic response. In the present problem, this approach can be utilized for current state simulations of the dynamic soil behavior, i.e., it is assumed that at the considered discrete time instant the increase of the soil stiffness due to compaction is negligible, and thus, in the simulation the soil properties are assumed to be linear elastic. The dominant modes of the soil, which is an infinite continuum, depend heavily on the specific vibratory excitation frequency, and they are a priori unknown. Thus, in a first step modal analysis is conducted to derive all modes of the continuum in a certain frequency range. Subsequently, from the entire mode set the modes that dominate the dynamic steady state response to a specific periodic excitation are identified, utilizing the maximum elastic strain energy per mode U_i in the steady state. The strain energy of the i-th mode, U_i, is defined as

$$U_i = \frac{1}{2} k_i q_i^2 \tag{1}$$

where k_i is the i-th modal stiffness, and q_i the i-th modal coordinate.

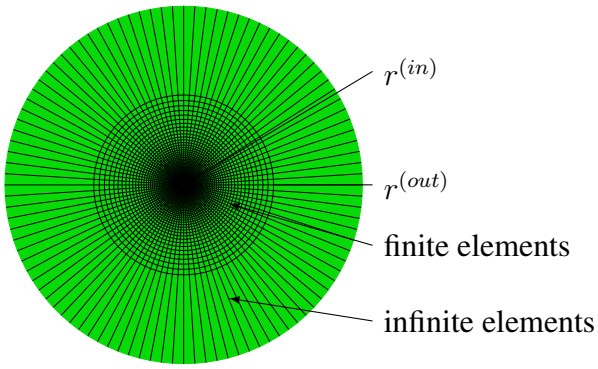

Figure 2: Spatial domain for the modal analysis.

In the present study, this approach is adopted upon a simple two-dimensional representation of the vibro-soil system, see Fig. 2. The soil is modeled as an annular planar plate of radius $r^{(out)} = 12\,\mathrm{m}$ with an circular hole of radius $r^{(in)} = 0.15\,\mathrm{m}$. A linear elastic homogeneous material with Young's modulus of $20\,\mathrm{MPa}$, Poisson ratio of $1/3$, void ratio of 0.735 and a dry skeleton density of $2650\,\mathrm{kg\,m^{-3}}$ is assigned to the plate. This material represents loose granular soil. Material damping according to Rayleigh with a ratio of critical damping $\zeta = 0.05$ at frequencies of $40\,\mathrm{Hz}$ and $72\,\mathrm{Hz}$ is used. The vibro excitation is simplified as a concentrated force rotating with a frequency of $60\,\mathrm{Hz}$ along the inner boundary of the soil plate in radial direction. The plate is spatially discretized by means of finite elements (FE) with a structured mesh of 100 four-nodes-full-integrated bilinear elements (CPE4) distributed along the circumference, as shown in Fig. 2. For the infinite continuum outside of the plate domain infinite elements (CINPE4) are used. Plane strain condition perpendicular to the excitation direction is assumed. The numerical model exhibits in total $13\,800$ degrees of freedom. The analysis is conducted by the FE software Abaqus 6.13-2 and it represents a linear perturbation step, also referred to as current state simulation.

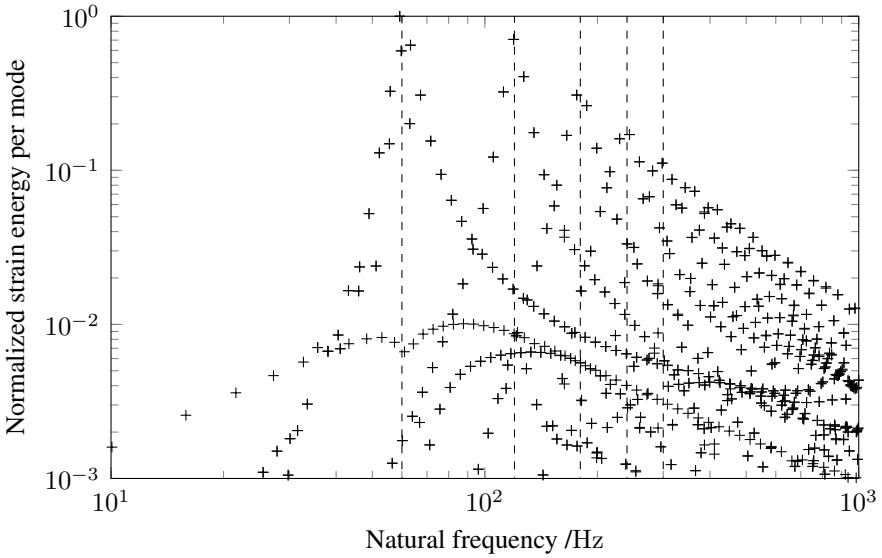

Figure 3: Normalized maximum elastic strain energy per mode for 13600 modes (detail).

As a result of the analysis, Fig. 3 displays for $13\,600\,\mathrm{modes}$ the maximum elastic strain energy per mode of the discretized planar soil continuum subjected to harmonic vibratory excitation as a function of the corresponding natural frequency up to $4230\,\mathrm{Hz}$. The vertical dashed lines indicate the excitation frequency of $60\,\mathrm{Hz}$ and multiples of it, i.e. $120\,\mathrm{Hz}$ and $180\,\mathrm{Hz}$. It is readily observed that there is no single isolated dominant mode, and modes clustered around 60, 120 and $180\,\mathrm{Hz}$ contribute the most to the dominant modes. This behavior is a result of the specific excitation, as subsequently outlined. At fixed location $(r^{(in)}, \phi)$ (with $r^{(in)}$ denoting the radius of the inner hole and ϕ the angel in cylindrical coordinates), the inner surface is subjected to a force excitation according to a Dirac comb δ ,

$$f_i\left(r^{(in)}, \phi, t\right) = \sum_{n=0}^{\infty} \delta\left(t - nT - t_0\right)\delta_{ir} \tag{2}$$

with phase time delay $t_0 = \phi T/2\pi$ (T denotes the excitation period) at the boundary to realize a spatial continuous force distribution. Symbol δ_{ir} denotes the Kronecker symbol. Fourier transformation of this expression,

$$F_i\left(r^{(in)}, \phi, \omega\right) = 1/T \sum_{n=0}^{\infty} \delta\left(\omega - n/T\right) e^{-j\omega t_0}\delta_{ir} \tag{3}$$

with $j = \sqrt{-1}$ reveals that spectral lines at multiples of the excitation frequency, n/T, occur. This is even true for an arbitrary force distribution $g\left(\tilde{t}\right)$ with $0 \leq \tilde{t} \leq a\,(\leq T)$, as exemplary shown in Fig. 4, where $g\left(\tilde{t}\right)$ is depicted at two fixed locations of the inner surface of the hole. For such arbitrary distributed force, the force excitation in the time reads as

$$f_i\left(r^{(in)}, \phi, t\right) = g\left(\tilde{t}\right) * \sum_{n=0}^{\infty} \delta\left(t - nT - t_0\right)\delta_{ir} \tag{4}$$

with the corresponding Fourier transformation

$$F_i\left(r^{(in)}, \phi, \omega\right) = G\left(\omega\right) 1/T \sum_{n=0}^{\infty} \delta\left(\omega - n/T\right) e^{-j\omega t_0}\delta_{ir}\ . \tag{5}$$

Symbol $*$ denotes the convolution. These relations not only hold true for continuous signals but also for discrete ones. The periodization of the signal with period T in the time domain by means of the discrete Fourier transformation is reflected in the frequency domain by spectral lines equally spaced with $1/T$. Thus, in Fig. 3 the maximum modal strain energies are clustered around these spectral lines.

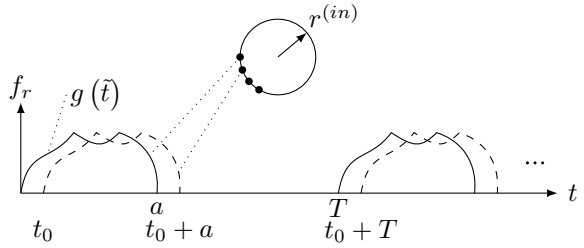

Figure 4: Rotating force excitation according to an arbitrary force distribution along the inner radius of the planar soil section.

In Fig. 5 the first to forth and the 15th and 16th most dominant mode shape are shown. The modes depicted in Figs 5(a) and (b) describe a translational motion of the inner boundary, and thus, the soil is subjected to a dominant shear distortion. This behavior is in agreement with the observation that the most effective compaction is related to shear distortion [10]. Due to the symmetric geometry of the numerical model, the eigenvalues come in pairs, and the corresponding mode shapes are rotated to each other but are otherwise identical. According to Figs 5(c) and (d), the hole of the planar soil section is elliptically deformed. In comparison between Fig. 5(c), (d) the mode shapes shown in Figs 5(e) and (f) represent higher modes compared to the previously discussed ones, and thus, the shape of the hole deflection is also of higher order.

Figure 6 shows the cumulative maximum elastic strain energy $S\,(n) = \sum_{i=1}^{n} U_i$ as a function of n, with $i = 1$ denoting the mode representing the largest strain energy, $i = 2$ the mode with the second largest strain energy, and so on. This figure shows that the increase of the modal strain energy becomes gradually smaller with increasing i. The first $200\,\mathrm{most}$ dominating modes (i.e. $1.4\,\%$) contribute to $80\,\%$ of the strain energy of all $13\,600\,\mathrm{modes}$. Thus, approximation of the system response using a modal analysis technique based on the most dominant modes identified from this figure significantly reduces the number of degrees of freedom without significant loss of accuracy.

3 DYNAMIC RESPONSE SIMULATION OF THE VIBRO-SOIL SYSTEM BASED ON A PLANAR MODEL

In the previous section, a two-dimensional planar soil section model subjected to a rotating force along the inner boundary has been used to describe vibrator-soil interaction. This modeling strategy cannot capture the physical processes at the vibro-soil interface. Thus, in a more elaborate approach according to [12], subsequently the soil is modeled as a three-dimensional planar annular soil section and the vibrator as a rigid cylinder body, as shown schematically in Fig. 7.

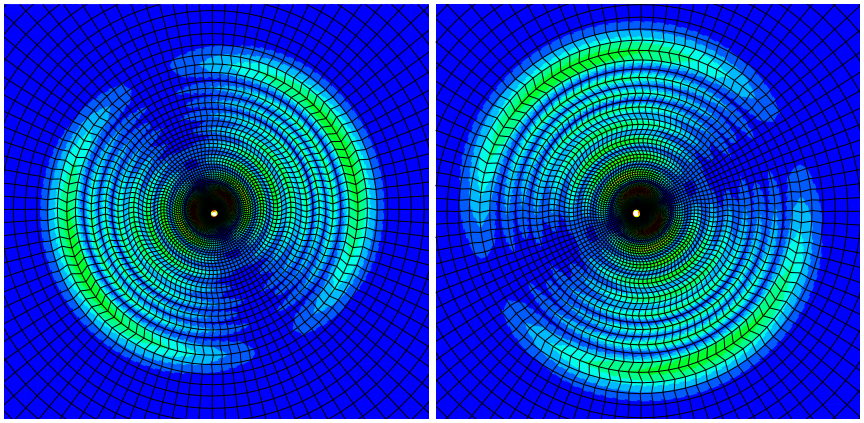

(a) First dominant mode shape with natural frequency of $59.20\,\mathrm{Hz}$.

(b) Second dominant mode shape with natural frequency of $59.20\,\mathrm{Hz}$.

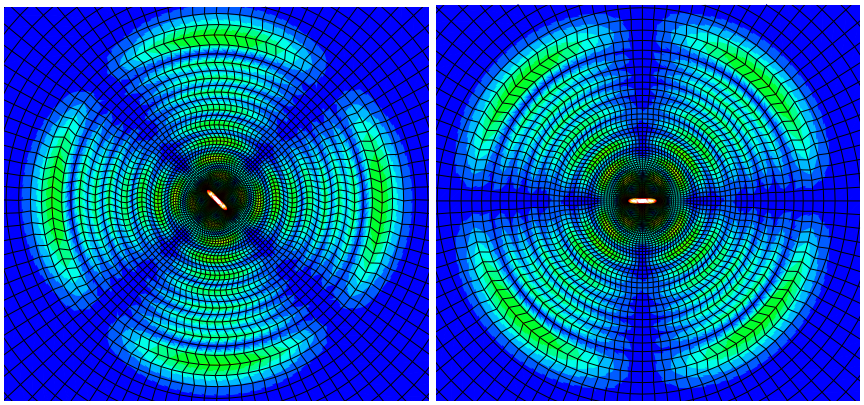

(c) Third dominant mode shape with natural frequency of $119.36\,\mathrm{Hz}$.

(d) Fourth dominant mode shape with natural frequency of $119.36\,\mathrm{Hz}$.

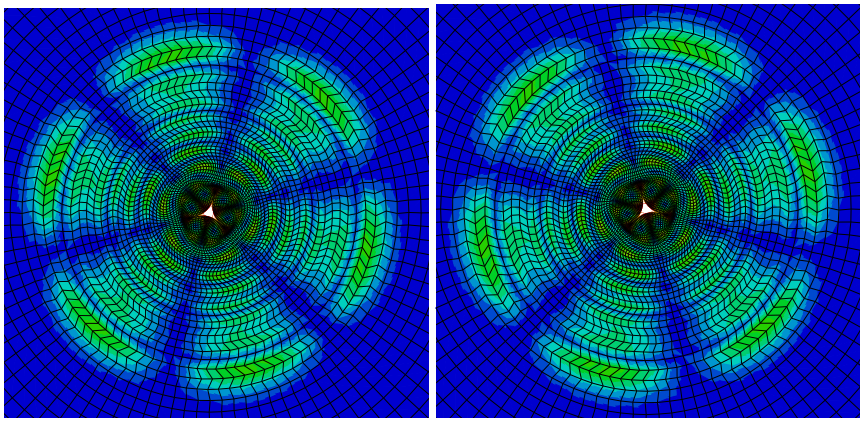

(e) 15^{th} dominant mode shape with natural frequency of $176.05\,\mathrm{Hz}$.

(f) 16^{th} dominant mode shape with natural frequency of $176.05\,\mathrm{Hz}$.

Figure 5: Selection of dominant mode shapes, sorted by the maximum of elastic strain energy per mode criterion in steady state. The contour indicates the norm of the corresponding eigenvalues.

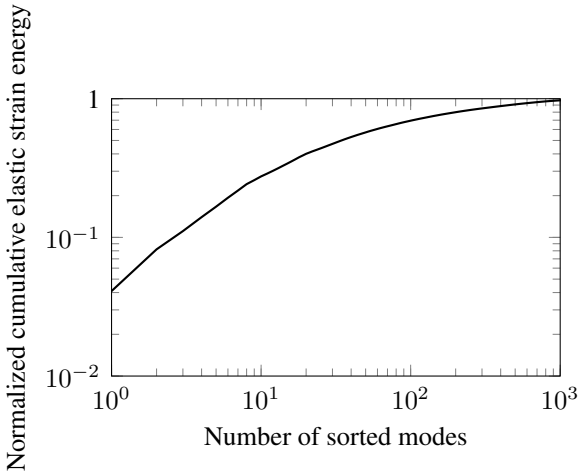

Figure 6: Normalized cumulative elastic strain energy.

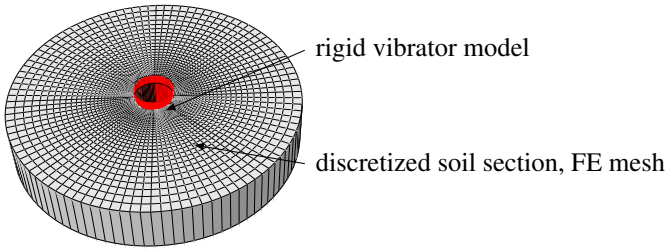

Figure 7: Model of the vibro-soil interaction system (detail).

The model of the annular soil continuum has the same dimensions and material properties as the one of the previous section, however, a thickness of $0.5\,\mathrm{m}$ is assigned. The upper and lower horizontal surface of the soil section is subjected to the vertical geostatic pressure at a depth of $15\,\mathrm{m}$, and at the outer radius the displacements are fixed. The rigid vibrator model has a lumped mass m of $2592\,\mathrm{kg}$ and a mass moment of inertia of $1662\,\mathrm{kg\,m^2}$ (with respect to the centroid). The adjacent surfaces of this rigid body and of the soil stay in full or partial contact, depending on the excitation frequency. In the simulation of the motion, for this "contact pair" the "surface to surface" algorithm implemented in the FE analysis software Abaqus is applied. The soil domain is discretized by means of 7102 eight-nodes-full-integrated elements (C3D8) from the Abaqus element library, arranged in a structured mesh, see Fig. 7. The maximum number of degrees of freedom of this model is $42\,006$, depending on the actual contact state between soil surface and vibrator. In reality, the motion of the vibrator is induced by an eccentric mass rotating with prescribed angular velocity of frequency ν. In the present simulations, the effect of this rotating eccentric mass is captured by a rotating in-plane centrifugal (radial) force $\mathbf{F}$, applied at the centroid of the rigid vibrator model. Force $|\mathbf{F}| = m_u e \nu^2$ is composed of the squared angular velocity ν^2 times eccentric mass m_u times eccentricity e, with $m_u e = 1.59\,\mathrm{kg\,m}$ for the considered vibrator. The tangential force component (Coriolis force), which is proportional to the angular acceleration, is neglected, because for slightly varying excitation frequency it is negligible small compared to the centrifugal force, and for steady state motion it

vanishes.

The results of the parametric study with a series of different excitation frequencies $\nu/2\pi$ ranging from 30 to $60\,\mathrm{Hz}$, spaced with $3\,\mathrm{Hz}$, are presented in Figs 8 to 12. As first outcome, the phase delay between the excitation force and the vibro-displacement shown in Fig. 8 is discussed. In this figure each graph represents the phase angle for a discrete excitation frequency specified at the right hand side of the figure in ascending order from the bottom of the circular marker. The horizontal axis represents time t normalized with respect to excitation period $T = 2\pi/\nu$. It is readily observed that after application of the force the phase angle increases sharply. Subsequently, the steady state solution is obtained after 10 to 20 (excitation) periods, depending on the excitation frequency. However, for excitation frequencies of 30, 33, 36 and $39\,\mathrm{Hz}$ the steady state is not reached during the predefined simulation time. For the lowest excitation frequency of $30\,\mathrm{Hz}$, at the end of the observation time the phase angle is about $60°$. With increasing excitation frequency this value gradually increases, and finally for the largest frequency $\nu/2\pi = 60\,\mathrm{Hz}$ it is already about $160°$. According to Fig. 9 resonance is attained between $\nu/2\pi = 30$ and $33\,\mathrm{Hz}$.

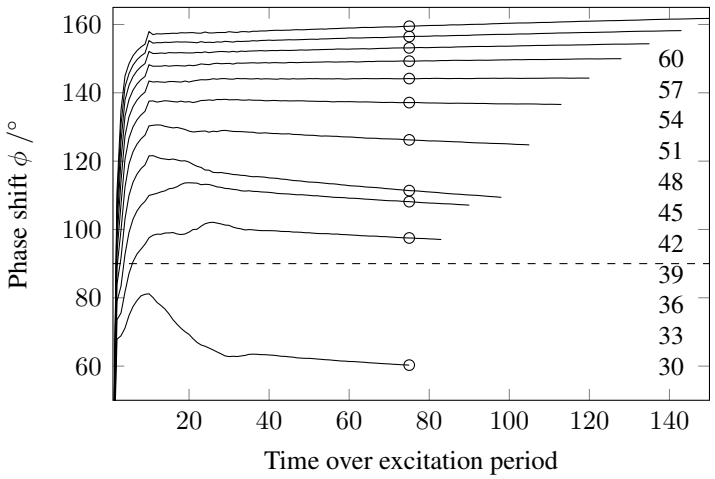

Figure 8: Phase shift between the centrifugal force and vibrator displacement.

The vibro-displacement is non-proportional to the excitation force (which is itself proportional to the square of the excitation frequency), as revealed by the displacement amplitudes depicted in Fig. 9. The largest amplitudes are related to an excitation frequency of $\nu/2\pi = 42\,\mathrm{Hz}$, and the lowest to $\nu/2\pi = 30\,\mathrm{Hz}$. The contact area normalized with respect the full area of the circular hole (i.e. full contact) shown in Fig. 10 is less sensitive to the excitation frequency sensitivity than expected. At the end of the observation time, the normalized contact area is between 0.38 (for the lowest considered frequency) and 0.28 (for the largest frequency).

As a further result, Fig. 11 shows the so-called eccentricity of ellipse of an arbitrary selected soil node at the contact surface in steady state condition. The eccentricity of ellipse is a criterion of the rotational motion of the soil, and it is calculated according to $\sqrt{a^2 - b^2}/a^2$, with a and b denoting the semi-major axis respectively the semi-minor axis of the elliptic soil node displacement. If the eccentricity is zero, the soil describes a circular motion. As expected, the eccentricity of the ellipse increases with increasing excitation frequency. However, the eccentricity values for frequencies 30, 33, 36 and $39\,\mathrm{Hz}$ are not representative because in these cases the outcomes are based on non-stationary transient response, as discussed before (see, for instance,

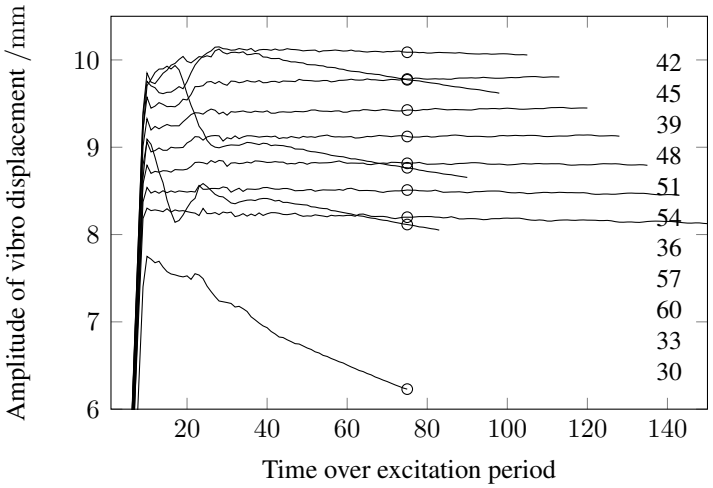

Figure 9: Amplitude of vibro displacement.

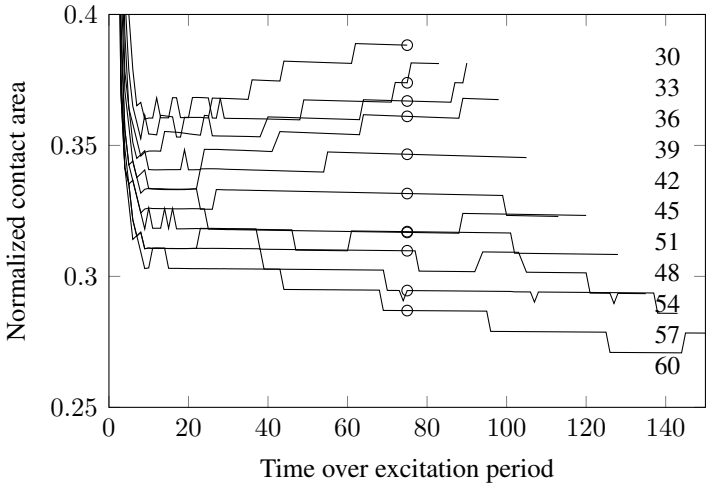

Figure 10: Normalized contact area.

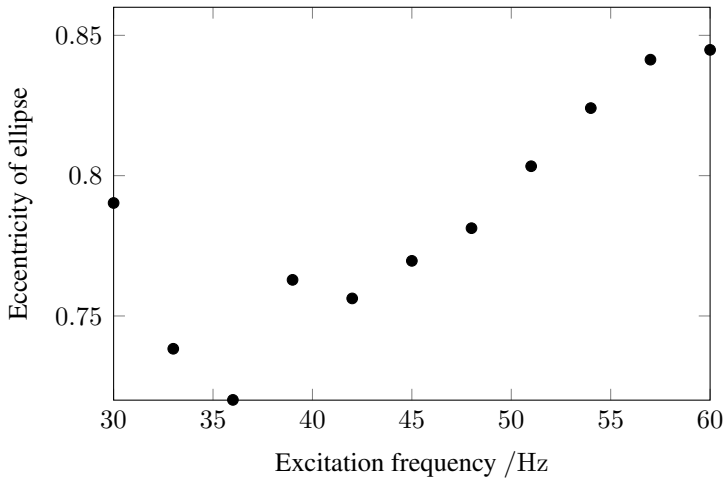

Figure 11: Eccentricity of ellipse of a soil node on the contact surface due to different excitation frequencies.

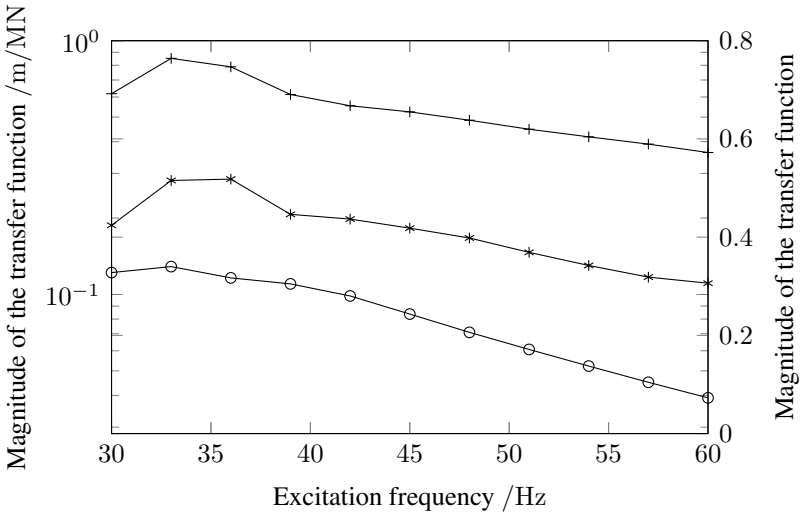

Figure 12: Magnitude of the transferfunction between centrifugal force and vibro displacement (circled markers) between vibro displacement and semi-major, respectively semi-minor axis (plus and asterisk markers).

Fig. 9).

The transfer function representing the ratio of force excitation and vibro-displacement in the frequency domain is shown in Fig. 12 by circular markers (dimension $\mathrm{m\,MN^{-1}}$). The vertical axis is logarithmic scaled. According to this function, the vibrator is at resonance between frequencies of $30\,\mathrm{Hz}$ and $33\,\mathrm{Hz}$. This is in agreement with the outcomes of Fig. 8 showing the phase delay between excitation and displacement.

The remaining graphs of this plot represent the transfer functions based on the ratio of vibro-displacement and the semi-major and semi-minor axis displacement components a respectively b of the considered soil node (none dimensional). An amplification in soil displacement due to the vibrator motion around $33\,\mathrm{Hz}$ is not as clear as in the before mentioned case. These transfer functions are almost affine.

4 IDENTIFACTION OF SOIL PROPERTIES BASED ON AN INVERSE MODEL

When appropriately equipped with sensors, the motion of the vibrator and its force exerted to the soil during deep vibratory compaction can be recorded. It is, however, difficult or even impossible to directly record the corresponding soil behavior and its densification. Thus, it would be desirable to deduce (respectively identify) from the vibrator response the evolution of the soil properties, applying a procedure referred to as inverse problem. For the solution of an inverse problem a simple mechanical model must be established, implying that this model responds in the same manner as the real system, which is in the present study the vibrator-soil interaction system. In contrast to a direct response simulation, the response of the real system, and thus, also of the mechanical model, is a priori known, and the parameters of the corresponding mechanical model are unknown. System identification aims at analyzing these model parameters based on the a priori known response.

In the subsequent study, the lumped parameter model shown in Fig. 13 [5] is assumed to describe appropriately the considered vibrator-soil interaction system. The given vibrator mass m is lumped, and the perpendicular arranged spring-dashpot systems with a priori unknown stiffness k and damper parameter c model the soil. The influence of the soil mass on the dynamic near field response is usually small, and thus, neglected. In general, the depicted system has two degrees of freedom, represented by the orthogonal displacement components in x- and y-direction. Since, however, the stiffness and damping are the same in both direction, and only the steady state response due to a force rotating with constant angular velocity is considered, the displacement of mass m is circular. Therefore, the orthogonal displacement components are the same with a phase shift of $\pi/2$, and consequently, the system has only one degree of freedom.

In a similar investigation, Fellin et al. [5] used the same model for identification of soil parameters based on the vibrator response recorded during *in-situ* vibratory compaction. In contrast, the present study uses *numerically* generated response data, derived by the simulations described in the previous section. This approach allows a validation of this system identification procedure, because the underlying data are based on a more elaborate model with well defined geometry and material properties.

Assuming harmonic excitation and steady state response, identification of time depending parameters k and c (respectively critical damping ratio $\zeta = c/(2\omega m)$ with $\omega = \sqrt{k/m}$) of the model shown Fig. 13 requires that the displacement amplitude A of the mass, excitation force $F = |\mathbf{F}|$, phase shift ϕ between excitation force $\mathbf{F}$ and displacement $\mathbf{u}$, and angular excitation frequency ν are known. In such steady state condition, stiffness k and damping parameter c can

be expressed in closed form as a function of A, F, ν, and ϕ [5],

$$k = \frac{F}{A}\sin\phi \quad , \quad c = \frac{F}{\nu A}\cos\phi \tag{6}$$

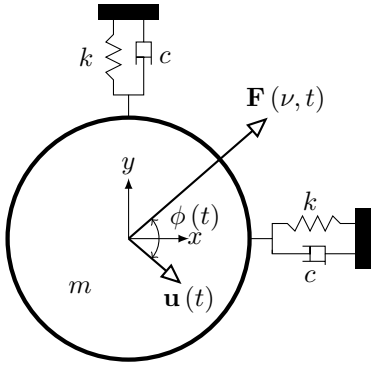

Figure 13: Simplified mechanical vibrator-soil interaction model used for system identification.

After identification of k and c, the relationship of the cone model of Wolf [19] is used to map the lumped stiffness k into Young's moduli E of the soil, Poisson μ ratio is assume to be known,

$$k = \frac{E r^{(in)}}{2\left(1-\mu^2\right)}\left(3.1\left(\frac{2d}{r^{(in)}}\right)^{0.75} + 1.6\right) \tag{7}$$

assuming rectangular contact between soil and vibratory, i.e. thickness d of the planar soil section times the radius of the vibratory $r^{(in)}$, as described in [4]. This assumption is, however, not supported by the results of the numerical simulation in the previous section, where the contact area according to Fig. 10 is less than $50\,\%$ of the total area.

Equation 6 is fed with the outcomes of the numerical simulations presented in the previous section, and subsequently Eq. 7 solved for Young's modulus E of the soil. In Fig. 14(a) the ratio of predicted modulus to actual modulus of the underlying numerical model is depicted with respect to normalized time (time t over excitation period T) for various excitation frequencies. It is observed that the predicted Young's modulus is about $60\,\%$ less than the actual one. However, the results indicate that at excitation frequencies close to resonance, i.e. 30, 33, 36 and $39\,\mathrm{Hz}$, Young's modulus can be predicted more accurately. Since for these frequencies the steady state response was not reached, additional studies are required to support this statement. The identified critical damping ratio ζ is between 0.22 ($60\,\mathrm{Hz}$ excitation frequency) and 0.4 ($33\,\mathrm{Hz}$ excitation frequency), and depends more on the excitation frequency than the predicted Young's modulus, see Fig. 14(b). The observed "fluctuations" in parameters E and ζ possibly arise from numerical instabilities of an ill-posed problem [8].

The absolute value $|\mathbf{R}|$ of the resulting model contact force $\mathbf{R}$ between the vibrator and the soil surface in steady state,

$$\mathbf{R} = k\mathbf{u} + c\dot{\mathbf{u}} \tag{8}$$

with the steady state displacement vector

$$\mathbf{u} = A\begin{pmatrix} \sin(\nu t + \phi) \\ -\cos(\nu t + \phi) \end{pmatrix} \tag{9}$$

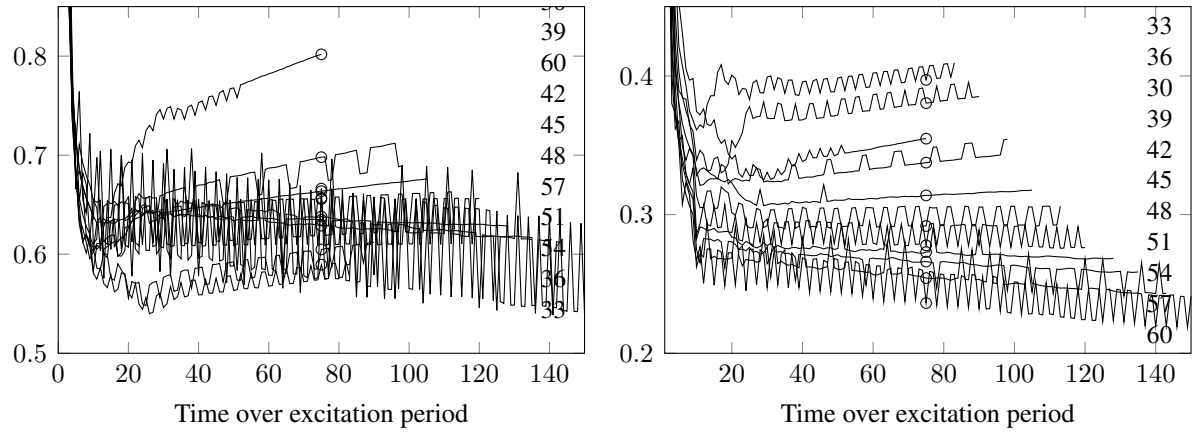

(a) Normalized Young's moduli (b) Ratio of critical damping

Figure 14: Results of the inverse model to reproduce (a) the Young's moduli and (b) the ratios of critical damping. The Young's moduli were normalized by this target value.

can be expressed as [4]

$$|\mathbf{R}| = A\sqrt{k^2 + (c\nu)^2} \tag{10}$$

Substituting the identified parameters k and c into this expression yields the contact force based on the lumped parameter model. Figure 15 shows for three excitation frequencies specified in the figure caption the identified contact force normalized with respect to its peak value. The dashed lines refer to the normalized forces as outcome of FE simulations, and the continuous graph refer to the normalized forces of the lumped parameter model according to Eq. 10. It is observed that both normalized forces are in the entire observation time both quantitatively and qualitatively in close agreement.

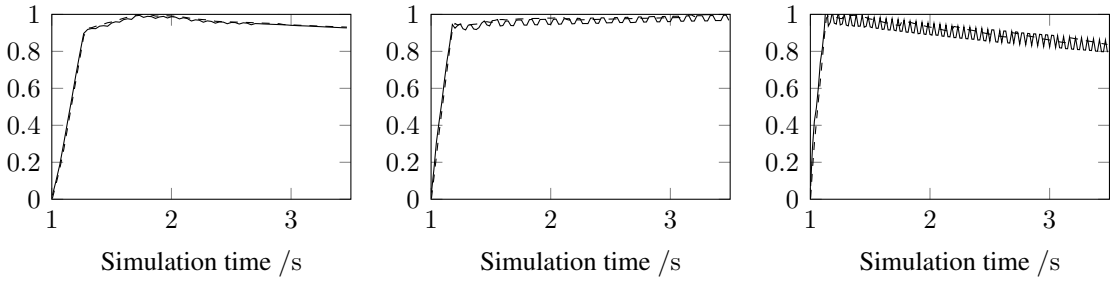

(a) 30 Hz of excitation frequency. (b) 45 Hz of excitation frequency. (c) 60 Hz of excitation frequency.

Figure 15: Normalized contact force as outcome of FE analysis (dashed line) and based on the fitted lumped parameter model according to Eq. 10 (continuous line).

5 SUMMARY, CONCLUSIONS, AND OUTLOOK

In this paper numerical modeling of deep vibratory compaction has been addressed. In the first study modal analysis delivered the natural frequencies and mode shapes of a crude annular

two-dimensional finite element (FE) model of the compacted soil. The most dominant modes excited by a rotating concentrated force were determined, based on the peak elastic strain energy per mode criterion in steady state condition. It was shown that the corresponding mode shapes are subjected to significant shear distortion, an observation that is in agreement with effective soil compaction. When taking into account only the most dominant modes, modal decomposition reduces significantly the computation costs of numerical response prediction of the interacting vibrator-soil system in a current state simulation. In such approach to be solved in future research, soil compaction can be modeled by changing the natural frequencies and mode shapes at discrete time instants during a transient modal analysis.

The second part of this paper aims at describing vibrator-soil interaction by means of a simplified FE model in terms of a three-dimensional elastic planar circular soil section subjected to a rigid rotating cylinder. Contact between soil and rigid cylinder has been simulated using an appropriate contact formulation.

In the third part the outcomes of the latter numerical study serve as input for system identification of soil parameters and contact force based on a simple lumped parameter model.

Despite the modeling efforts described in the literature and in this paper, simulation of deep vibratory compaction is still a challenging and in many aspects unsolved problem. Further research should take into account the influence of pore water and fluid flow injection, vertical cyclic vibrator motion and nonlinear constitutive behavior to reveal the most relevant physical processes during deep vibratory compaction. Based on such studies, it should be possible to create physically more meaningful and more reliable simplified models describing the compaction process.

6 ACKNOWLEDGEMENT

The research described in this paper has been partially funded by the Austrian Research Promotion Agency (FFG) through the project GeoGlueStrengthening within the framework of the FFG Program EraSME (846136). This support is gratefully acknowledged.

REFERENCES

[1] D. Adam, *Continuous compaction control with vibratory rollers* (in German). Dissertation. TU Wien, Vienna, 1996.

[2] M. Arnold, I. Herle, Comparison of vibrocompaction methods by numerical simulations. *International Journal for Numerical and Analytical Methods in Geomechanics*, **33**(16), 1823–1838, 2009.

[3] R. Cudmani, T. Meier, V Osiney, Development of a numerical model for the prediction of densification of cohesionless soils during deep vibratory compaction. In H. Gonin, Holeyman A., F. Rocher-Lacoste eds. *Symposium International sur le Vibrofoncage et la Vibrocompaction (TRANSVIB 2006)*, pp. 131–140, Paris, France, September 21-22, 2006.

[4] W. Fellin, *Rütteldruckverdichtung als plastodynamisches Problem* (in German). A.A. Balkema, 2000.

[5] W. Fellin, G. Hochenwarter, A. Geiß, On-line Verdichtungskontrolle bei der Rütteldruckverdichtung (in German). *Bauingenieur*, **75**(9), 607–612, 2000.

[6] D.A. Greenwood, Vibrational loading used in the construction process, In M.P. OReilly, S.F. Brown eds. *Cyclic loading of soils: from theory to design*, chapter 10, pp. 434–475, Blackie and Son Ltd., 1991.

[7] FFG Program EraSME, *GeoGlueStrengthening*, project no. 846136, 2014–2017.

[8] J. Hadamard, *Lectures on Cauchy's problem in linear partial differential equations.* Courier Corporation, 2014.

[9] T. Hamann, S. Henke, J. Grabe, Numerische Modellierung der Verdichtung rolliger Boeden mittels Impulsverdichter, Rütteldruckverfahren und Rüttelbohle (in German). In D. Adam, R. Herrmann eds. *Baugrundverbesserung in der Geotechnik*, Institut für Geotechnik der Universität Siegen, Germany, September 14-15, 2010.

[10] I. Herle, Influence of pressure level and stress amplitude on the compaction of granular soils. In D. Kolymbas, W. Fellin, eds. *Compaction of Soils, Granulates and Powders*, Vol. 3 of Advances in Geotechnical Engineering and Tunneling, pp. 285–295, 2000. A.A.Balkema.

[11] Keller Grundbau GmbH, *Die Tiefenrüttelverfahren* (in German), Brochure, 10-02D.

[12] S. Kessler, G. Heibrock, T. Triantafyllidis, On prediction of vibrocompaction performance using numerical models. In H. Gonin, Holeyman A., F. Rocher-Lacoste eds. *Symposium International sur le Vibrofoncage et la Vibrocompaction (TRANSVIB 2006)*, pp. 233–242, Paris, France, September 21-22, 2006.

[13] M. Killeen, *Numerical modelling of small groups of stone columns*. Dissertation, National University of Ireland, Galway, 2012.

[14] K. Kirsch, K. Kirsch, *Ground improvement by deep vibratory methods.* CRC Press, 2016.

[15] M. Nendza, *Untersuchungen zu den Mechanismen der dynamischen Bodenverdichtung bei Anwendung des Rütteldruckverfahrens* (in German). Dissertation, Technische Universität Braunschweig, 2007.

[16] G. Qiu, S. Henke, J. Grabe, Application of a Coupled EulerianLagrangian approach on geomechanical problems involving large deformations. *Computers and Geotechnics*, **38**(1), 30–39, 2011.

[17] A.A. Rodger, Vibrocompaction of cohesionless soils. *Cementation Research Limited*, Internal Report, R.7/79, 1979.

[18] J. Wehr, Variation der Frequenz von Tiefenrüttlern zur Otimierung der Rütteldruckverdichtung (in German). *Mitteilungen des Fachgebiets Grundbau und Bodenmechanik*, Vol. 38, pp. 67–77, 2005.

[19] J.P. Wolf, *Foundation vibration analysis using simple physical models*. Pearson Education, 1994.

[20] H. Yu, *Cavity Expansion Methods in Geomechanics.* Springer Science+Business Media, 2000.